Boletín Geológico

SERVICIO GEOLÓGICO COLOMBIANO

Boletín Geológico, 51(1), 2024

https://doi.org/10.32685/0120-1425/bol.geol.51.1.2024.680

Received: September 27, 2022

Revision received: April 22, 2024

Accepted : June 26, 2024

Published on line: June 30, 2024

Research article

Deciphering the modern stress field facies in Costa Rica and vicinity from earthquake focal mechanisms and GNSS support

Descifrando las facies modernas del campo de esfuerzo tectónico en Costa Rica y vecindad mediante mecanismos focales de terremoto y apoyo GNSS

Allan **López-Saborío**[1] [2], Luis Alejandro **Carvajal-Soto**[1]

[1]Universidad Latina de Costa Rica, Escuela de Ingeniería Civil, San José, Costa Rica.

[2]GeoTec S.A, Consultor independiente, Cartago, Costa Rica.

RESUMEN

Se recopila una base de datos de 2547 mecanismos focales de terremotos para modelar el campo de esfuerzo tectónico en Costa Rica, sur de Nicaragua y norte de Panamá. Se determinan 86 tensores regionales de esfuerzo. La orientación general del esfuerzo horizontal máximo (SH Max) es subparalela a la dirección de convergencia N 32° E de la placa de Cocos con la placa Caribe a lo largo de la fosa mesoamericana, con una rotación horaria de +- 20° por debajo de los 30 km de profundidad. Se identifican tres órdenes de esfuerzos: el primero debido al movimiento absoluto de la placa de Cocos, el segundo generado por la interacción triple de esta con las placas Caribe y Nazca, y el tercero debido a contrastes de densidad impuestos por las cordilleras volcánicas, ígneas y sedimentarias activas y paralelas a la fosa, las cuales en combinación con fallas regionales y sus interacciones, actúan en conjunto como deflectores de los esfuerzos tectónicos locales que rotan hacia el norte y oeste. Los datos GNSS observados y modelados del campo de velocidades horizontales, orientados al NNE, presentan una correlación notable con las direcciones del SH Max interpoladas en la capa superior. Estas características, junto con las permutaciones locales y regionales de los ejes del elipsoide de esfuerzos, explican las interacciones de los regímenes tectónicos y sus complicaciones neotectónicas. Se genera un escenario 2D-3D detallado con límites sismo tectónicos realistas y más objetivos, utilizando categorías de regímenes de esfuerzo junto con la relación tectónica R'. Los resultados tienen aplicación práctica en estudios de amenaza y riesgo sísmico, exploración de recursos naturales.

Palabras clave: mecanismos focales, inversión, tensor de esfuerzo, permutación, órdenes del esfuerzo.

ABSTRACT

A database containing 2547 earthquake focal mechanisms from Costa Rica, southern Nicaragua, and northern Panama is analyzed to model the modern tectonic stress field through inversion. 86 regional stress tensors are derived, revealing the general orientation of the maximum horizontal stress (SH Max) to be sub-parallel to the N 32° E convergence direction of the Cocos plate with the Caribbean plate along the Middle America Trench. A clockwise rotation of approximately ±20° is observed below 30 km depth. Three orders of stress are identified: the first attributed to the absolute motion of the Cocos plate, the second characterized by high magnitude boundary forces from the triple interaction of the Cocos plate with the Caribbean and Nazca plates, and the third due to density contrasts imposed by trench-parallel active volcanic, igneous, and sedimentary mountain ranges. These features, combined with regional faults and their interactions, deflect the local tectonic stress north and westward. Observed and modelled GNSS data of the NNE-oriented horizontal velocity field correlate well with the direction of interpolated SH Max in the upper layer. These findings along with the local and regional permutations of the stress axes ellipsoid elucidate the interactions of tectonic regimes and their neo-tectonic complications. A detailed 2D-3D scenario is generated, offering realistic seismotectonic boundaries using stress regime categories and the tectonic R' relationship. The results hold significant practical implications for seismic hazard and risk assessment, as well as the exploration and exploitation of natural resources.

Keywords: focal mechanism, inversion, stress tensor, permutation, stress orders

Citation: López-Saborío, A. Carvajal-Soto, L.A. (2024). Deciphering the modern stress field facies in Costa Rica and vicinity from earthquake focal mechanisms and GNSS support). Boletín Geológico, 51(1). https://doi.org/10.32685/0120-1425/bol.geol.51.1.2024.680

1. INTRODUCTION

The modelling of the stress field has gained a strong input during the last decades thanks to the work implemented by the World Stress Map Project community (https://www.world-stress-map.org/). A worldwide database is under continuous updating and the latest 2016 edition contains more than 42.870 entries which are the input for applied detailed maps in contrasting geotectonic settings, specialized documents, and research guidelines. Plenty of software was developed to assist the investigations and many specialized publications emerged to testify the rather coherent output and the explanations for regional and local behaviors of the stress field. A concise vocabulary and legend evolved, and stress field research is now a well-established scientific discipline that involves many specialized fields with a wide range of applications both in the industry and academia.

The releases of the World Stress Map Project have clearly demonstrated the existence of plate-scale first-order, the regional or second order and the local third order stress fields which are controlled by plate boundary forces, intraplate stress sources (mountain belts and glacial rebound) and active faults, local inclusions, detachment horizons and density contrasts, respectively.

The modelling of the stress field is of primordial importance for a coherent interpretation of the tectonic forces, strain accumulation and deficits interacting with existing geological faults and the generation of new ones and their types, all of them being vital inputs supplements for the seismic hazard studies, along with the fault-slip and dilation tendencies of local and regional faults. The stress field is also applied in the geo-engineering analysis of rock masses proposed to host underground civil infrastructure, assist in the interpretation of mineral deposits emplacements and the factors controlling the behaviors of oil, gas, and geothermal drilling and related borehole stability and management of associated reservoirs.

In this paper, the results of previous works by Montero and Morales (1990), López (1999) Quintero and Güendel, (2000), are noticeably upgraded and updated with a much larger data set and studied with state-of-the-art analytical tools and methods to unravel the particular stress conditions of Costa Rica, northern Panamá and southern Nicaragua. They are examined and analyzed in detail as a contribution to the World Stress Map, the ISRM Commission on stress and earthquakes and to the Kuk-Ahpán project, which is studying the structure and the lithosphere of Central América and their implications in the seismic hazard and risk. Also, as an input for related fields of applied research.

1.1 Objectives

The main goal of this work is to decipher the properties and characteristics of the modern stress field by calculating the associated tensors, deduced from focal mechanisms, to explain the ongoing deformations at different crustal layers. The central objective is to detect the orders of stress variability in 3D and even the potential overlapping and coexistence of stress regimes within relatively small domains, where the maximum horizontal stress (SH Max) develops complicated patterns at the local scale. All these attributes are reflecting the complex seismotectonic of a region affected by past, recent and present-day interactions of the Cocos-Caribbean and Nazca plates (COCANA). The detailed genetic link among stress and regional structural styles is not addressed here since it requires lengthy discussions, and it is focused on another study. This paper contributes to a better understanding of the interactions among these blocks, which are partially responsible, for the generation of the contemporaneous stress field and the crustal deformation (Carvajal-Soto *et al.*, 2020).

The product is the Costa Rica stress map constrained by the guidelines and quality ranking system of the WSM. As stated by Montone *et al.* (2004), these maps depict the active stress conditions at areas where the data are sparse, as is the case in some regions of Costa Rica, and they contribute to understand the relationship between active stress, past tectonic setting, neotectonics and seismicity.

2. PREVIOUS WORKS

Previous works on the determination of the tectonic Stress Field in Costa Rica from focal mechanisms (FM) include those by Montero and Morales (1990), López (1999, 2012), López *et al*. (1992, 2011), Quintero and Güendel (2000). The first authors used a small population of focal mechanisms kinematic axes, Quaternary volcanic vents, and recent geomorphic uplifts in an attempt to study its general features. The second introduced the calculations of tectonic stress tensors at different geodynamic and crustal levels, with more data and used the quality ranking system of the WSM, to check and model the acting stress directions in a geotectonic setting controlled by the interaction of the abovementioned plates. The third main research depicted a concise database of new events and presented their stress determinations. Camacho (2003) have studied the seismotectonics of the Panamá Fracture Zone (PFZ).

At the regional scale (Arcila and Muñoz, 2020) presented a well-documented study displaying the characteristics of the stress field which is currently operating within the Colombian territory and neighboring regions, ending precisely in the SW limit of the

region herewith analyzed. In that context this work is the logic continuation to the west with a small overlapping.

2.1 Seismotectonic setting

Costa Rican crust is relatively small but complicated and lies in a complex geotectonic setting directly affected by the interaction of the COCANA plates (figure 1), where active vulcanism and tectonics are very well developed. The Cocos plate (COP) subducts beneath the Caribbean Plate (CAP) along the 5 Ma old Middle America trench (MAT) at a velocity of 8.5-9.0 cm a-1 in the NW and SE, respectively, with a mean direction of ~N32°E (De Mets *et al*. 1994; Protti *et al*. 1996). The scenario is further intricate in southern Costa Rica-northern Panamá, where the triple junction of the Nazca-Cocos-Caribbean plates interact along the Panamá Fracture Zone (PFZ). This right lateral N-S oriented transform fault moving at 5.5 cm/yr., creates a complex and very active seismotectonic setting (DeMets,2001). Marshall *et al*. (2000), analyzed with details the Kinematics of diffuse faulting across the western Panama block into Costa Rica, finding a systematic stress-strain arrangement with sub-parallel orientation to the Cocos-Caribbean plates convergence direction. The effects of the subduction erosion along the MAT convergent margin, its associated quaternary tectonics and their relation to volcanism, were studied by Ranero and Von Huene (2000), and Von Huene *et al.* (2000). They detected a significant influence of Quaternary convergent margin tectonics by the subducting lower plate along the MAT which accommodates three distinct types of oceanic crust. Their influence on continental margin structure is most prominent in the middle and upper slope regions. Notably, erosion is more pronounced where the Cocos Ridge and its associated seamounts subduct, in contrast to the stable slope where smooth lower plate subduction occurs as in NW Costa Rica. Upper plate features aligned with lower plate segment boundaries extend inland for more than 120 km from the trench axis and correspond to volcanic arc segmentation, while the extent of faulting associated with ocean plate flexure adjacent to the trench axis shows a strong parallelism.

Among the crustal stress volumes herewith analyzed there is a transition from subduction of normal to thickened oceanic crust (Arroyo *et al*., 2014), which is particularly developed in the southern rough domain of the COP. There, the long chains of submarine inactive volcanic seamounts cordilleras, some as high as 2000 m (Figure 1) coming from the Cocos-Nazca spreading center, are being subducted along the MAT producing important amounts of seismicity and are acting also as individual indenters, whose combined effects explains several regional deformation zones (López, 1999). The COP coupling zone is larger in the southern segment than in the Nicoya Peninsula (NP) (Carvajal-Soto *et al*, 2020), where the sea bottom created at the East Pacific rise contains the Cocos Ridge, inducing major subduction earthquakes along a lower subduction angle than in the NP with a relatively large recurrence period (~40 years) for its highly destructive events. The PFZ appears also as a weak boundary as discussed ahead. Figure 1 shows these aspects and the most important epicenters up to 2020.

Morell (2016) has integrated and correlated the vital link among subduction erosion, ridge, and transform subduction with fluid flow release, deformation, seismogenesis and volcanism, parameters which are fundamental to properly understand and evaluate the sources of the acting and recent stress field. A clear time-dependent along strike relation was proven between scales of upper plate deformation and localized shortening with the sea bottom asperities and thickness of the inboard subduction of the Cocos plate.

Carvajal-Soto *et al*. (2020) reported that the elastic interseismic crust deformation is produced by interactions along block interfaces, where the high north eastward convergence rate of COP, and moderate to high coupling ratios, produce a compressive pattern in Nicaragua, Costa Rica, and the western Panamá.

3. DATA AND METHODS

3.1 Data

The previous database of FM, moment tensors and their parameters (López,1999) have been triplicated and now consist of 2547 events, covering as from 1924 to 2021, collected from Global Centroid Moment Tensor Project- CMT, International Seismological Center-ISC, GeoForschungsZentrum-GFZ, solutions along with those from the local networks in Costa Rica, Red Sismológica Nacional-RSN and Observatorio Sismológico y Vulcanológico de Costa Rica-OVSICORI. Other several published data sources are shown in the references, among them the events by Güendel (1986), Quintero and Güendel (2000), Chaves *et al.* (2017), Arroyo and Linkimer (2021). This significant increase is a consequence of the extended coverage of the local seismic networks, their instrumental performance, relative longer observation periods and improved analytical tools. The region considered in the database containing the focal solutions is shown in Figure 2, where it is evident that those events closely related to or influenced by the ongoing subduction process along the MAT and COCANA prevail among the rest, despite of their epicenter and hypocenter locations.

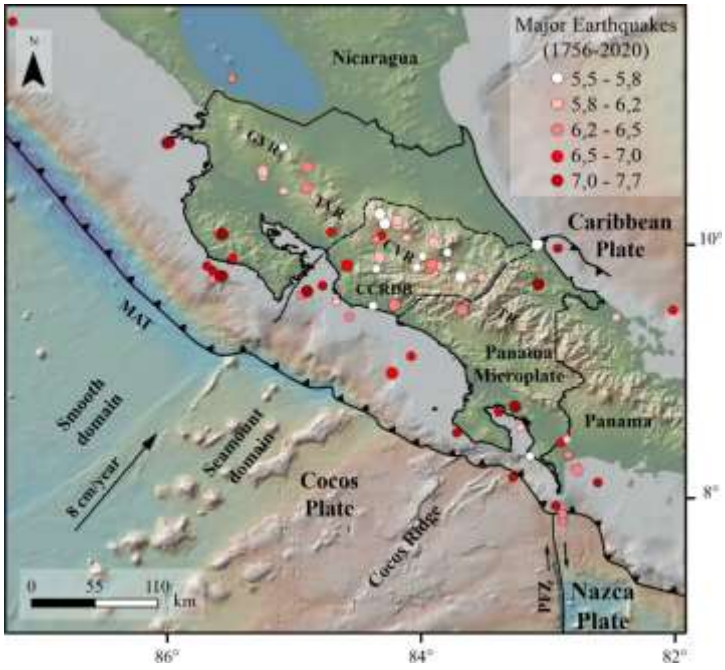

Figure 1. Plate tectonic environment of Costa Rica and epicenters of major earthquakes 1756-2020. Modified from Linkimer *et al* and RSN. GVR is the Guanacaste Volcanic Range, TVR the Tilarán Volcanic Range, CVR the Central Volcanic Range, CCRDB is the Central Costa Rica Deformed Belt. PFZ is the Panamá Fracture Zone, the limit between the Cocos and Nazca plates.

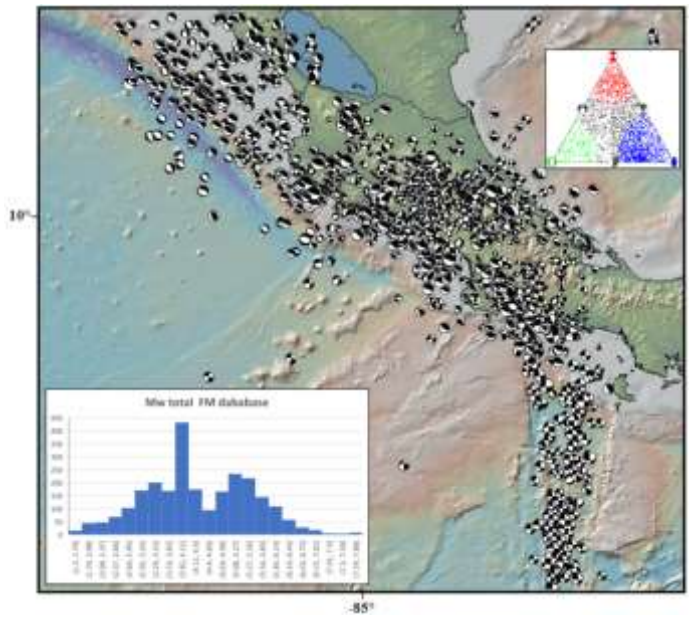

Figure 2. Histogram for the 2547 FM total population reported in Annexed 1. The column heights are proportional to the abundance of Mw, and it increases from left to right. Despite the dispersion the presence of two main groups with medium to intermediate magnitudes are recognized, while those with Mw larger than 6.5 up to 7.6 are the minority. Central Costa Rica presents more events due to better coverage by the local seismological networks although the rest of the country is monitored by several hundred stations. In the triangle classification the vertices represent pure normal, thrust, and strike-slip focal mechanisms and the intermediate regions their relative kinematic variability. It displays the overall seismic complexity with every type of tectonic regime well developed.

Those and other domains which present individual characteristics are herewith analyzed. Annexed 1 contains the orientation parameters of the compiled and reformatted database for each focal mechanism along with their dates in a single format, coordinates, depth, Mw, calculated Maximum (SHmax) and minimum (sh min) horizontal stress directions, regime index, regime code sensu WSM and source; and, annexed 2 contains the distribution of depths and magnitudes of the seismic database.

Then, the criteria to delimit the sub-volumes within each of the three crust layers, was the distribution of SH Max and its depth variability, their tectonic regimes and the other WSM cited parameters in conjunction with local and regional clustering of FM. The spatial distribution of P and T axes was implemented as proxy to delineate a very general stress scenario at the regional scale and is justified as follows.

The upper layer down to 15 km depth is the most deformed and as depicted in figure 3-A, covers the entire studied region with all the possible types of focal solutions for their 1146 FM. Despite this kinematic complexity shown by the scatter of the P axes, an important part displays a clear NNE-SWW orientation in agreement with and subparallel to the general trend of deformation imposed by the COP absolute motion. T axes reveal a larger scattering imposed by the normal and transtensive FM.

The intermediate layer covers the depths from 16 to 30 km resembling at some extent the kinematics of the previous one, but as shown by the P and T stereograms of their 990 FM, their scattering is reduced and accompanied by a tendency to rotate clockwise. The same applies to the T axes and the overall scenario is corroborated in the classification triangle, where the distensive plots are less abundant while the compressive and strike-slip tend also to concentrate relatively in Figure 3-B.

The deeper layer, figure 3-C, contains 357 FM and starts at 31 km depth with a clear dominance and influence of the subduction processes along the MAT and transcurrency at the PFZ, but with less activity in the latter than in the upper layers.

The scenario for events with magnitudes higher than 6.0 for all depths, 166 in total, is rather selective with reverse focal solutions concentrated dominating the MAT and its direct influence regions as well as in the back-arc thrust and fold belt. The strike-slips control the PFZ but are also present in central Costa Rica and southern Nicaragua with transpressive and transtensive components while normal events are related to down-dip environments. This confirms again the predominance of NE compression as portrayed in the P and T stereograms with strong clustering of their poles also present in the triangle.

3.2 Stress Inversion and stress regimes.

The stress field tensors were calculated by the application of the Win Tensor program by Delvaux (https://damiendelvaux.be/Tensor/tensor-index.html), which implements the methodology devised by Angelier (1975, 1984) and applies the WSM criteria to this challenging task, which must be applied with care in order not to apply it in a mechanical way to avoid incoherent results. The background for stress inversions is based on the premise that from a group of closely spaced FM, assumed to be generated by a spatially and time invariant homogeneous stress field, where one of the nodal planes slips in the direction of maximum resolved shear stress, it is possible to calculate the stress tensor responsible for the displacement of the majority of the involved seismic faults. This situation is solved by a mathematical inversion which minimizes the difference between the measured rake angle of the active plane and the theoretical one calculated by this process (Delvaux and Barth, 2010). There are several strategies to solve this so-called inversion problem, attending the mechanical conditions that the shear and normal stress magnitudes and the shear stress direction of the nodal planes are controlled by four of the six parameters of the complete stress tensor. The result is a reduced tensor which calculates the principal stress axes $\sigma1 > \sigma2 > 3$ and their shape or radio of principal stresses $R = (\sigma2-\sigma3/\sigma1-\sigma3)$ fluctuating from 0 to 1. Bott (1959) proposed the parameter R (stress differences) to classify stress regimes. It provides valuable information on the shape of the stress ellipsoid and specially on its stability and tendency to permutate its axes and migrate on time and space from a given stress regime to another, when the R value is closer to 1 or 0.

There is no need to select a priori which of the nodal planes is the active fault, since both are theoretically activated by the same stress tensor and calculations using separate groups render very similar results. Then the true nodal plane can be determined by means of frictional criteria.

To generate a fine tuning of the spatial distribution of the deformation, the stress regime index R', tool developed by Delvaux *et al.* (1995), was used due to its simplicity to overcome the limitations of the R, in which two distinct regimes may have the same value. R' is a modification of R and is expressed in a continuous range from 0 to 3 as follows:

R' = R for normal faulting regime
R' = 2-R for strike-slip regime
R'= 2+R for thrust faulting regime

0 and 3 represent radial extension and radial compression, 0.5 and 2.5 uniaxial extension and compression, 1.0 and 2.0 transtension and transpression, 1.5 strike-slip, respectively. R' was applied to the entire FM population to better describe and analyse the variability of the faulting regimes generated by the acting stress tensors.

4. RESULTS

Several FM populations located within close spatial proximity were selected according to the WSM criteria and inverted, generating a total of 86 representative stress tensors, 54 corresponding to the upper layer, 23 to the intermediate one, and 9 to the deepest crust.

The inversion also identifies the true nodal plane according to the friction angle assigned during the process. This determination was applied to every sub-domain at each layer; and as an example, an FM cluster in SE Costa Rica during 2018, reported by Arroyo and Linkimer (2021), is shown in Figure 4. The calculated tensors are very similar despite both nodal planes are used or those separated according to their friction.

In general, the tensors at all depths depict a good correlation with known structural arrays and domains. During a preliminary run the dimensions of each sub-domain were adjusted as to contain enough input data to assure a reliable and coherent stress inversion and allow spatial separation of acting tensors. This criterion was further supported by the map plotting and the interpolation of the SH Max and WSM parameters, as discussed ahead.

4.1 Stress state in the upper layer.

The upper layer down to 15 km depth is the most brittle and deformed and as depicted in Figure 5, containing the FM epicentral location and the selected sub-domains, covers the entire studied region with all the possible type of focal solutions. Every kinematic motion is well represented by abundant populations as shown by the classification triangle without any dominance, which is also confirmed also by orientation diagrams of the scattered 54 σ1 and σ3 axes generated by the inversions. The detailed parameters of each tensor and related properties are presented in Table 1. Note the very acceptable ranges of tensor qualities sensu WSM and the existence of several unknown regimes.

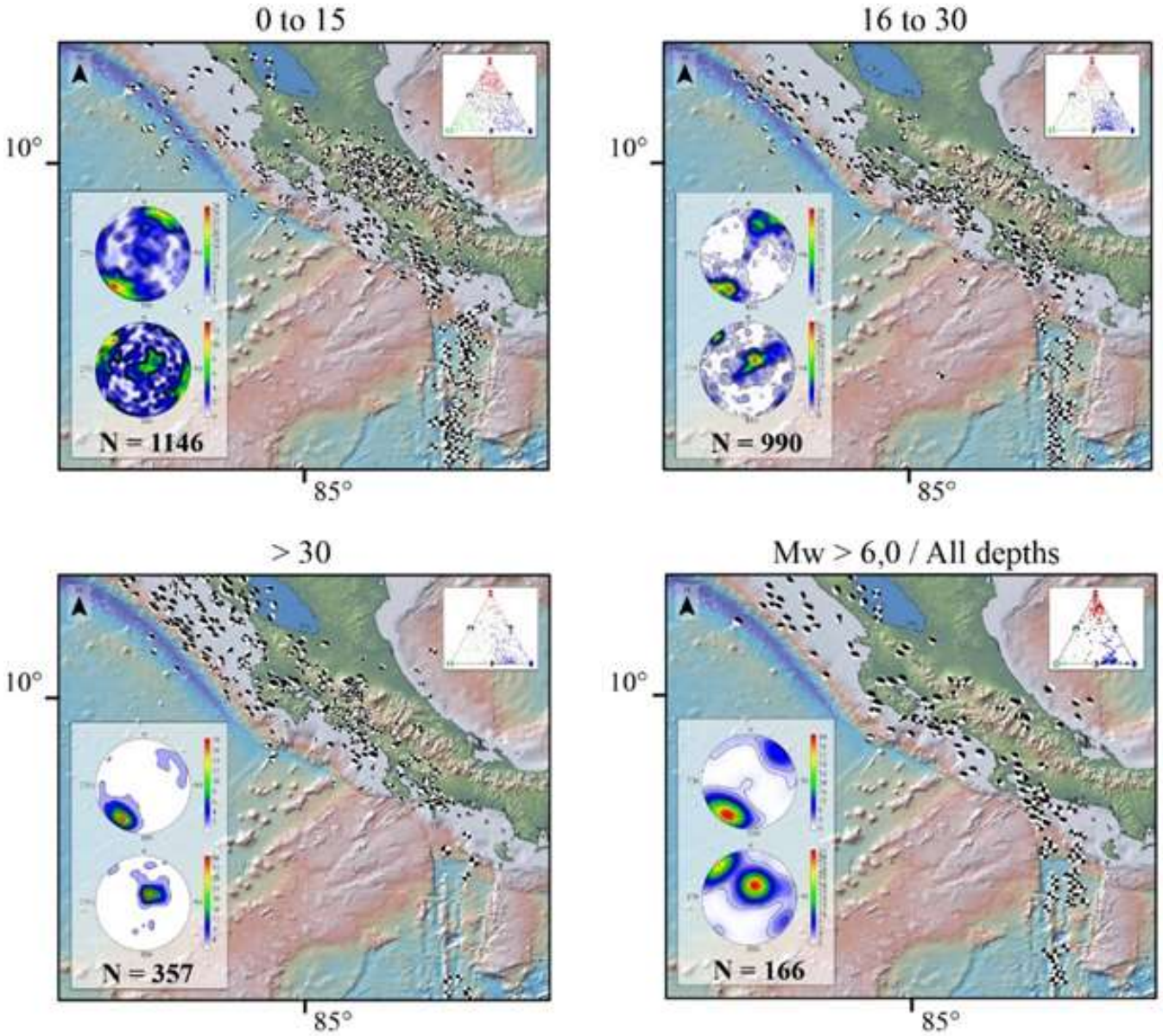

Figure 3. Focal mechanism maps for every defined crustal layer and one for only the events with Mw higher than 6,0. The insets are the contoured P and T axes stereograms depicting the heterogeneity of the stress field. Compare with figures 5, 6 and 7 where only the σ1 and σ3 of the correspondent stress tensors are plotted.

4.2 Stress state in the intermediate layer.

In general, the response of this layer to the interaction of the acting plates is similar to the upper one, although seismicity is relatively less developed in some particular regions, like the PFZ and its north prolongation into the continent, central Costa Rica and the Caribbean. Thrusting, strike-slip prevails with subordinated normal faulting within a wide range of orientations as from north to east, as shown by σ1 and σ3 axes from 23 tensors in Figure 6. The proportion of tensors with qualities A, B, and C is prominent in Table 2.

4.3 Stress state in the deeper layer.

This lower layer is relatively more stable than the ones above analyzed and some of its seismicity and associated FM tend to concentrate in some clusters, but the majority is dispersed. The stress tensors obey only to strike-slips and thrusting events rotated clockwise with respect to the intermediate and shallowest layers as shown in Figure 7. The related parameters are displayed in Table 3.

Table 1. Parameters of the stress tensors determined for each sub-domain within the upper crust layer.

Sub-vol	σ1	σ2	σ3	R	R'	Qwsm	n/N	Regime
U-1	34/1	124/06	299/84	0.27	2.27	B	10/92	TF
U-1	211/10	051/79	301/04	0.53	1.47	B	13/92	SS
U-1	059/33	161/18	274/51	0.52	0.52	C	6/92	UF
U-1	253/45	137/24	028/35	0.68	0.68	B	10/92	UF
U-1	211/01	310/86	121/04	0.29	1.71	B	23/23	SS
U-2	208/01	113/81	298/09	0.43	1.57	A	78/596	SS
U-2	198/11	289/02	029/79	0.51	2.51	A	52/596	TF
U-2	061/05	316/71	152/18	0.51	1.49	A	31/298	SS
U-2	357/11	152/78	266/05	0.56	1.44	A	27/596	SS
U-2	296/00	184/89	026/01	0.61	1.39	B	20/596	SS
U-2	216/60	052/29	318/07	0.37	0.37	A	15/137	NF
U-2	068/40	164/06	261/49	0.44	2.44	A	15/139	UF
U-2	216/60	052/29	318/07	0.37	0.37	A	15/137	NF
U-2	068/40	164/06	261/49	0.44	2.44	A	15/139	UF
U-2	269/23	168/24	037/56	0.52	2.52	B	14/139	TF
U-2	315/52	054/06	148/37	0.44	0.44	B	12/139	UF
U-2	157/29	360/59	253/10	0.48	1.52	B	12/54	SS
U-2	092/25	295/63	186/10	0.62	1.38	C	18/27	SS
U-2	115/20	012/31	232/52	0.5	2.5	B	18/298	TS
U-2	084/74	192/05	283/15	0.46	0.46	B	12/298	NF
U-2	069/19	167/21	301/61	0.83	2.83	B	11/488	TF
U-3	035/04	205/86	305/01	0.54	1.46	A	22/22	SS
U-3	002/32	148/53	262/17	0.42	1.58	B	11/42	NS
U-3	053/05	207/84	323/03	0.52	1.48	B	9/42	SS
U-3	195/21	290/13	050/65	0.59	2.59	C	7/63	TF
U-3	086/37	325/35	206/34	0.6	0.6	C	7/63	XF
U-3	175/82	352/08	082/00	0.33	0.33	B	14/63	NF
U-4	027/01	296/33	119/57	0.38	2.38	B	10/22	TF
U-4	307/50	103/38	202/12	0.60	0.60	B	10/22	NS
U-4	026/01	296/09	122/81	0.04	2.02	A	18/44	TF
U-4	306/50	083/31	187/22	0.56	0.54	B	11/44	NS
U-5	035/05	143/75	304/14	0.02	1.79	B	28/32	SS
U-5	053/71	318/02	227/19	0.54	0.38	C	12/32	NF
U-6	211/04	301/02	053/85	0.13	2.13	B	35/38	TF
U-6	000/69	161/20	253/06	0.37	0.37	C	16/38	NF
U-7	021/06	266/75	113/14	0.09	1.91	B	57/69	SS
U-7	182/80	055/06	324/08	0.12	0.12	B	34/69	NF
U-7	311/02	220/42	043/48	0.44	0.44	C	31/69	TS
U-8	311/12	092/75	219/09	0.43	1.57	C	15/15	SS
U-9	205/18	112/10	355/70	0.66	2.66	C	7/9	TF
U-9	167/70	031/15	298/14	0.12	0.12	B	11/11	NF
U-10	291/44	082/42	186/15	0.33	0.33	C	6/22	NS
U-10	036/04	141/74	305/15	0.18	1.82	B	16/16	SS
U-11	312/40	104/46	209/14	0.67	1.33	C	6/12	NS

(Table 1. Cont.)								
Sub-vol	**σ1**	**σ2**	**σ3**	**R**	**R'**	**Qwsm**	**n/N**	**Regime**
U-11	239/26	345/30	116/49	0.61	2.61	B	9/12	TS
U-12	203/08	310/65	109/23	0.24	1.76	C	56/67	SS
U-12	274/20	179/13	057/66	0.40	2.40	B	10/67	TF
U-12	054/55	308/11	211/33	0.12	0.12	B	11/67	NF
U-13	027/02	279/82	118/07	0.09	1.91	A	22/28	SS
U-13	250/58	119/22	019/21	0.13	0.13	C	10/16	NF
U-14	033/01	126/71	303/19	0.25	1.75	B	21/21	SS
U-14	138/02	033/82	229/08	0.76	1.24	B	8/21	SS
U-15	035/05	143/75	304/15	0.18	1.82	B	28/40	SS
U-15	055/72	317/03	226/18	0.38	0.38	C	12/40	NF
U-16	040/07	135/36	300/53	0.22	2.22	B	20/20	TS
U-16	176/75	290/06	021/14	0.45	0.45	C	12/20	NF

Note: Parameters of the stress tensors determined for each sub-domain within the upper crust layer ranging from 1 to 15 km depth along with their quality sensu WSM. The R and R' stress shape ratios, the remaining population after the inversion and the determined stress regimes are shown. The quality ranking for the orientation of the SHmax stress indicator is termed A when SH is believed to be within ±15°, B when SH is within ±15-20°, C within ±20-25°, D for questionable SH orientation (±25-40°), and E with no reliable information (>±40°). Regime codes: NS normal fault, TF thrust fault and their combinations with SS strike-slip fault termed NS and TS. UF is the unknow regime according to Zoback (1992). These definitions apply also to tables 3 and 4. Note several volumes display coexisting tensors in all the tested layers.

Table 2. Results of the stress inversions performed in the intermediate layer.

Sub-vol	S1	S2	S3	R	R'	Qwsm	n/N	Regime
I-1	220/02	117/82	310/08	0.51	1.49	A	87/91	SS
I-1	061/80	169/03	259/10	0.97	0.97	B	8/91	NF
I-2	207/51	000/36	100/13	0.38	0.38	C	7/20	NS
I-3	202/24	299/15	058/61	0.45	2.50	B	100/100	TF
I-4	198/29	322/45	089/31	0.17	1.83	B	52/68	TS
I-4	251/17	158/12	033/69	0.95	2.95	A	20/68	TF
I-5	078/05	169/10	324/79	0.37	2.37	B	10/10	TF
I-6	218/06	128/01	025/84	0.57	2.57	A	25/41	TF
I-6	256/72	062/17	154/04	0.48	0.48	C	6/41	NF
I-6	138/15	260/64	042/21	0.43	1.57	C	6/41	SS
I-7	206/25	298/06	041/65	0.53	2.53	A	288/330	TF
I-7	148/30	257/30	022/45	0.82	2.82	A	32/288	UF
I-7	011/10	273/37	113/51	0.57	2.57	B	16/660	TS
I-7	049/34	199/53	309/14	0.67	1.33	B	9/20	NS
I-8	213/12	123/0	33/78	0.54	2.54	A	20/72	TF
I-8	297/70	123/20	32/2	0.47	0.47	B	8/2	NF
I-8	012/17	109/21	246/62	0.56	2.56	C	5/15	TF
I-9	218/6	310/14	105/75	0.66	2.66	B	12/30	TF

.

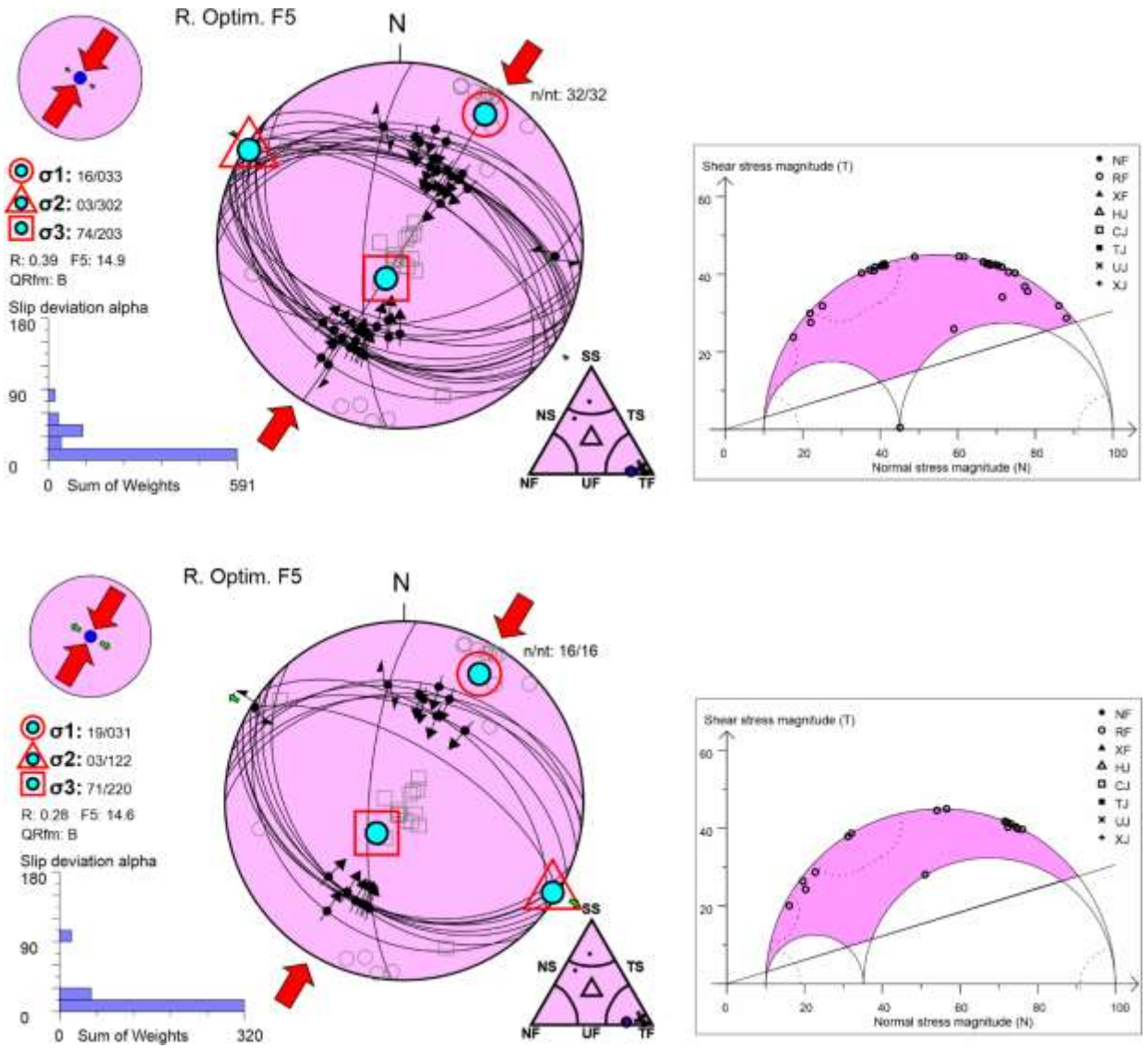

Figure 4. Example of selection of the true nodal plane choosing the plane with lower friction angle, which in theory should be the most prone to slip. The FM were reported by Arroyo and Linkimer (2021) and correspond to a seismic sequence in SE Costa Rica during 2018. Note the similarity of tensors either with both nodal planes or those separated according to their friction. Also, the predominant thrusting regime depicted in the triangular classification with two faults with strike-slip component being compatible with the acting tensor. In both cases their geomechanical feasibility is shown by the respective 3D Mohr diagrams.

5. DISCUSSION

5.1 Characteristics and properties of the stress field.

In this section the pattern of the stress field, its properties and characteristics are analyzed, with special attention to the kinematics and geometries of the FM, orientation of the SH Max and the variability of the stress ellipsoid shape as characterized by the R' factor. The latter two elements are fundamental to understand the recent, present, and future behaviors of regional structures and their tectonic regime transition. Such quantification of the stress distribution and their characteristics, especially in the plate interface, are fundamental for conjecturing megathrust earthquakes that may occur in the future (Saito & Noda, 2022), which in the past have been highly destructive within the studied region.

The stress inversions results demonstrate that the stress field in the Costa Rica sector of the Caribbean plate is not homogenous, and it is driven and strongly controlled by the interactions among that plate with the Cocos and Nazca plates. Heterogeneous stress fields are rather common and complicated by 2D/3D different large and medium responses to plate motions, lateral density contrasts and lithospheric flexures (Zoback, 1992; Heidbach *et al*., 2007; Kassaras and Kapetanidis, 2018).

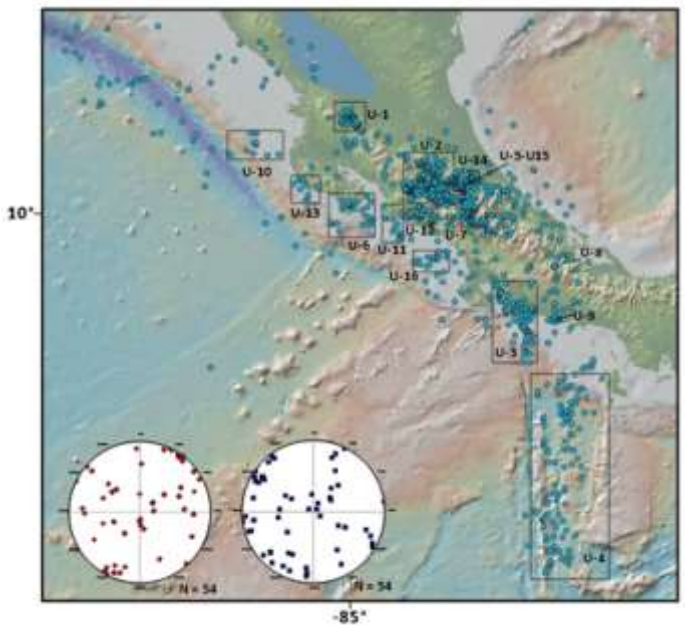

Figure 5. Locations of the inverted FM in the upper layer. Some regions display concentrations but were not considered for stress inversion due to their low magnitudes, only to display the SH Max. Sigma 1 are the red diamonds and sigma 2 the blue squares. σ1 (red diamonds) orientations of the 54 tensors are mainly directed to the NE, subparallel to the convergence of the Cocos-Caribbean plates and to the submarine inactive volcanic chains in the rough domain. NW oriented are also identified. Sigma 2 are the blue squares. Code and parameters of domains are displayed in Table1

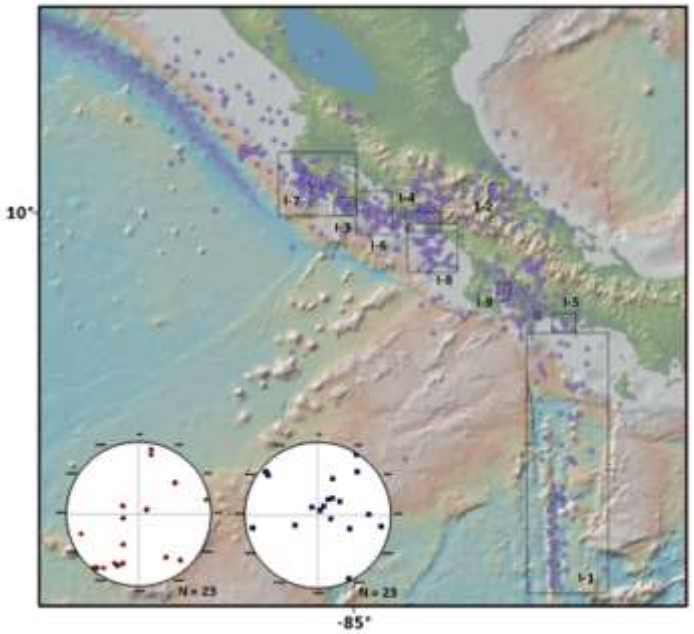

Figure 6. Domain location of the intermediate layer where 23 stress tensors for strike-slip, thrust and normal faults were determined. This layer is relatively less deformed than the upper one. Conventions as in Figure 5.

Table 3. Results of the stress inversions performed in the deepest layer.

Sub-vol	S1	S2	S3	R	R'	Qwsm	n/N
D-1	044/03	313/27	140/62	0.53	2.53	A	17/56
D-1	090/03	352/67	182/23	0.39	1.61	C	4/56
D-1	162/14	029/70	255/14	0.42	1.58	C	5/14
D-2	083/18	188/40	334/45	0.31	2.31	B	13/64
D-2	214/18	124/00	033/72	0.36	2.36	B	12/64
D-2	072/00	341/75	162/15	0.92	1.08	C	7/32
D-3	243/13	083/76	334/05	0.55	1.45	B	13/30
D-4	047/04	162/81	316/08	0.45	1.55	C	4/12
D-5	215/17	310/16	080/66	0.08	2.08	A	50/50

Note: Orientation data for the σ1, σ2 and σ3, R the stress ratio, R' the stress shape index, the WSM quality designation, the final population inverted after successive separations from the original FM dataset and the regime code sensu WSM.

High heat flow variations along MAT strike and enrichment and loss of fluids along the plate boundaries (Bangs *et al*., 2015), their hydraulic connectivity, and in general the influence of subduction fluids on pore pressure, are jointly contributing to the critically stressed state of the deforming lithosphere. Martinez Garzón *et al.* (2016) also draw attention to the sensitivity of stress inversion of FM to pore pressure changes. All these parameters and concerns should be taken into consideration in other investigations where tectonic stresses are analyzed. Due to the 3D proximity of important FM clusters the permutation-reactivation chances for re-rupturing the same fault patch increase. This condition especially applies where their planes interact inducing a complex homogeneous stress field but also could produce aseismic slip when heterogenous (Okamoto *et al*., 2022). As a consequence of the stress inversion results and the modelling of the SH Max general orientation, it is unmasked that its sub parallelism to the Cocos plate convergence direction is valid until the 30 km depth, then a clockwise rotation of ± 20° is detected.

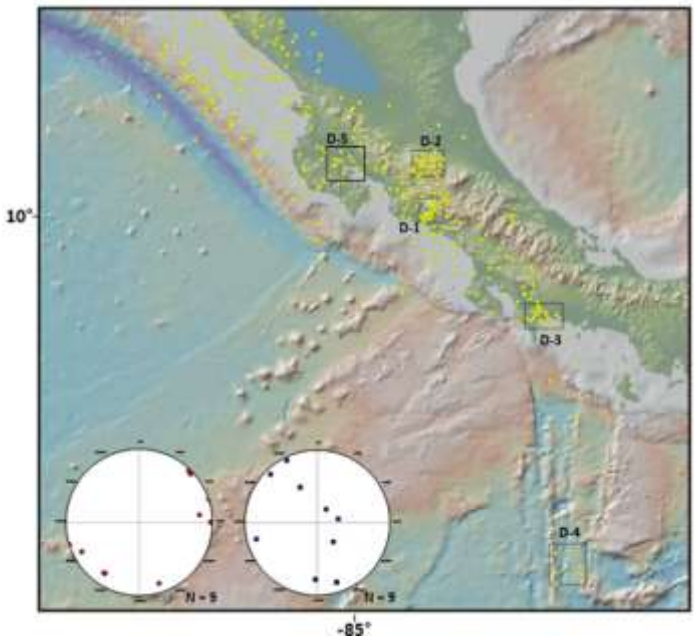

Figure 7. Orientation diagram for 9 FM sub-domains within the deeper stress layer. Note the diffuse seismicity and the very small population along and across the PFZ. Conventions as in Figure 5.

Dealing with the relation between FM and tectonic stress, it is important to take into account that since the seminal works of McKenzie (1969) and Michael (1987), it is recognized that their P, B and T axes are not equal to the σ1, σ2 and σ3 axes of the stress ellipsoid, although they can depict a broad picture of contraction and extension trends and can be used as their proxies. This situation is especially applicable when there is high friction contrast between the fault planes, usually very low, and higher in the host crust volume. They are equal only in the case of new faults formed within homogeneous bodies while for reactivated planes the difference can be as large as 20° for azimuth and plunge. Also, that a unique stress field is capable, given the proper geomechanical conditions, to reactivate fault planes or generate new ones with different directions, even if they are not well oriented to the stress field.

Accordingly in the present investigation the P and T axes are plotted to display the very general trends for compression and dilation directions and mainly to exhibit the trajectories of the SH Max at the regional scale, a common practice in the stress analysis, which is validated locally by the formal stress inversions of FM, applying the WSM guidelines.

The FM classification on triangular plots (figures 2, 3, 4, 5 and 6) clearly show variations with depth in the kinematics and relative presence of different faulting regimes. All types are well developed in the upper layer with abundant populations, but in the intermediate layer the normal, transtensive and transpressive events diminishes their development, while thrusting increases due to the compressive dominance of the subduction processes. For the same reason, in the deeper crustal layer, down below 30 km depth, such behaviour is increased and the distensive FM are notably reduced while the strike-slips also dimishes. In general, the MAT displays, at all seismogenic levels, thrusting accompanied by normal outer rise and down dip events, while the PFZ is characterized by a dominant group of dextral shears and subordinated transpressive and transtenssive events, along with a relatively small but representative population of normal FM.

The results also demonstrate that from the forearc to the back-arc across this sector of the Caribbean plate, the dominant kinematics and associated tensors correspond to thrust and strike-slips regimens. Even the latter extends to the San Andrés and Providencia Island in the northeastern Caribbean.

To fully understand the implications of the FM dataset properties for the objectives of this investigation it is necessary to consider that the database was not declustered (Martínez Garzón *et al*., 2016), so some local stress interactions and perturbations can be present. Those perturbations cannot be ignored and could explain the coexistence of different faulting regimes sensu WSM (figures 5, 6, 7) within small crustal volumes, although the leading tectonic regime is compressive. The prevailing condition is a predominance of thrusting and strike-slips across and along the local and regional crust, with isolated small regions of normal faulting. The maps of R' and the stress regime index discussed ahead (Figure 8) display those consistent attitudes at all the tested intervals and offer more contrast and details on the stress regimes variations at different depths.

One of the characteristics of the analyzed FM population is the relative lack of directional stability in the trends and plunges of their P-T axes. This is particularly noticeable in the shallowest layer, in which all types of kinematics and tectonic regimes sensu WSM are present, as shown in Figure 5. Its orientation diagram, although depicting a very clear concentration of P axes to the NE-SW with sub-horizontal inclinations, also contains a scatter of data that depart from this behaviour.

The respective P-T orientation diagrams are shown in Figure 3 for each studied layer and a consistent NE-SW clustering of the nearly horizontal P axes is present within the three scenarios. Dispersion is high in the upper layer, where every type of kinematics is present among the 1146 focal solutions and even normal and transtensive events are well represented by a close to vertical concentration of P axes along with the correspondent groups of vertical and steeply plunging T axes. At the intermediate layer, the mentioned dispersion is almost absent while the normal events are much less developed in the population of 990 FM.

Deepening across the layers, a consistent and increasing clockwise rotation of nearly 25 degrees in the P azimuth is detected while the respective T axes appear relatively fixed. It is worth mentioning that rotations of the stress axes related to strong seismic events have depicted shifts around 5 degrees, as in the case of the Nicoya big subduction earthquake Mw 7,6 in 2012, NW Costa Rica.

Table 1 and maps in Figures 3 and 5 indicate that some sub volumes in the upper layer contain characteristic and dominant tectonic regimes, as in the case of those located within or in the zones of direct influence of the MAT and the PFZ. In others, despite the concentration of events, there are overlapping regimes, which is explained by the spatial superposition of secondary and even tertiary stress orders. An example is the case of the CCR sub-volume, located in the central depression of Costa Rica, where compression and direction of the SH Max to the NE predominate, generated by compressive and strike-slip tensors, but which spatially contains normal, transpressive and transtressive events, as shown in Figure 3 in an area of approximately 5000 km2, those kinematics coexist. It should be considered that it has an excellent seismological coverage and is tectonically complex, being included within the northern boundary of the Panamá microplate.

5.1 R shape ratio, stress stability and permutation

Hu & Angelier (2004) characterized the stress permutations in brittle tectonics as the substitution of one of the principal stress axes by another one and recognized exchanges between the σ1 and the σ2 with high values of the R value or the σ2 with the σ3 with low values. Their origin is associated to the joint and interlinked actions of the heterogeneity of the brittle deformation and the anisotropy of the mechanical properties. The R= σ2- σ3/σ1-σ3 value is reported by the inversions and represented graphically by a 3D Mohr diagram (see figure 4), facilitating the identification of such permutations, which are widely developed in Costa Rica (López, 1999). The principal relative stress magnitudes vary from 0, where σ2 equals σ3, to 1, where σ2 equals σ1, while values around 0.5 reflect stable tensors and tectonic regime. Understanding of those mechanical scenarios offers light to interpret changes of reverse or normal faulting to strike-slip depending on the R value.

Since different stress regimes may have the same R value, the R' stress shape index (Delvaux *et al*., 1995) is applied to overcome that limitation. It also represents those transitions governed by the stress ellipsoid, but in a continuous range with extreme values from 0 to 3.00, covering all the scenarios from radial extension to radial compression. The same applies to the related identified stress regime classification corresponding to different R'. In figure 9, the R, R' and the tectonic regime histograms for each of the analyzed crustal layers clearly depicts the variety of stress ellipsoid shapes, especially for the shallowest one; most of them are not clustered around R=0.5 but display a wide range of values, a clear indication of tectonic instability and strong tendency to permutation. Even the UF unknown stress regime population, the one where the maximum horizontal stress is not properly defined according to the tectonic regime categories defined by Zoback (1992) and applied by the WSM, value 6 in the X axis, was detected.

The values of the stress regime and R' were interpolated in plan view to further analyse the adjustment of the faulting style values and the variations of the stress ellipsoid under the contemporaneous stress field. The A inset in Figure 8 corresponds to the upper layer, where strike-slip, transpression and thrusting dominate the tectonic scenario with isolated rims of transtension and normal faulting. At the intermediate layer, inset B, the distension increases along the Guanacaste volcanic range (GVR in Figure 1), but it is accompanied by transpression and strike-slip with an important increase of trusting in relation to the previous layer, in both cases governed by the ongoing subduction process. UF situations are more relevant in different tectonic settings. At the deeper setting, from 30 to 60 km depth and deeper, pure strike-slip and its transition to transtension and transtension is by far the most prominent strain attribute and it is strongly developed along the PFZ, decreases at some extent in the Caribbean plate but becomes more developed in the surroundings of the MAT, specially at the NW. The insets D, E and F present the variation in R' along the three-layer crust with a dominance of transtension, strike-slip and transpression with some local pockets of radial and uniaxial compression. The R' are highest only in a few localities within the upper layer along and close to the MAT, also at the Caribbean platform.

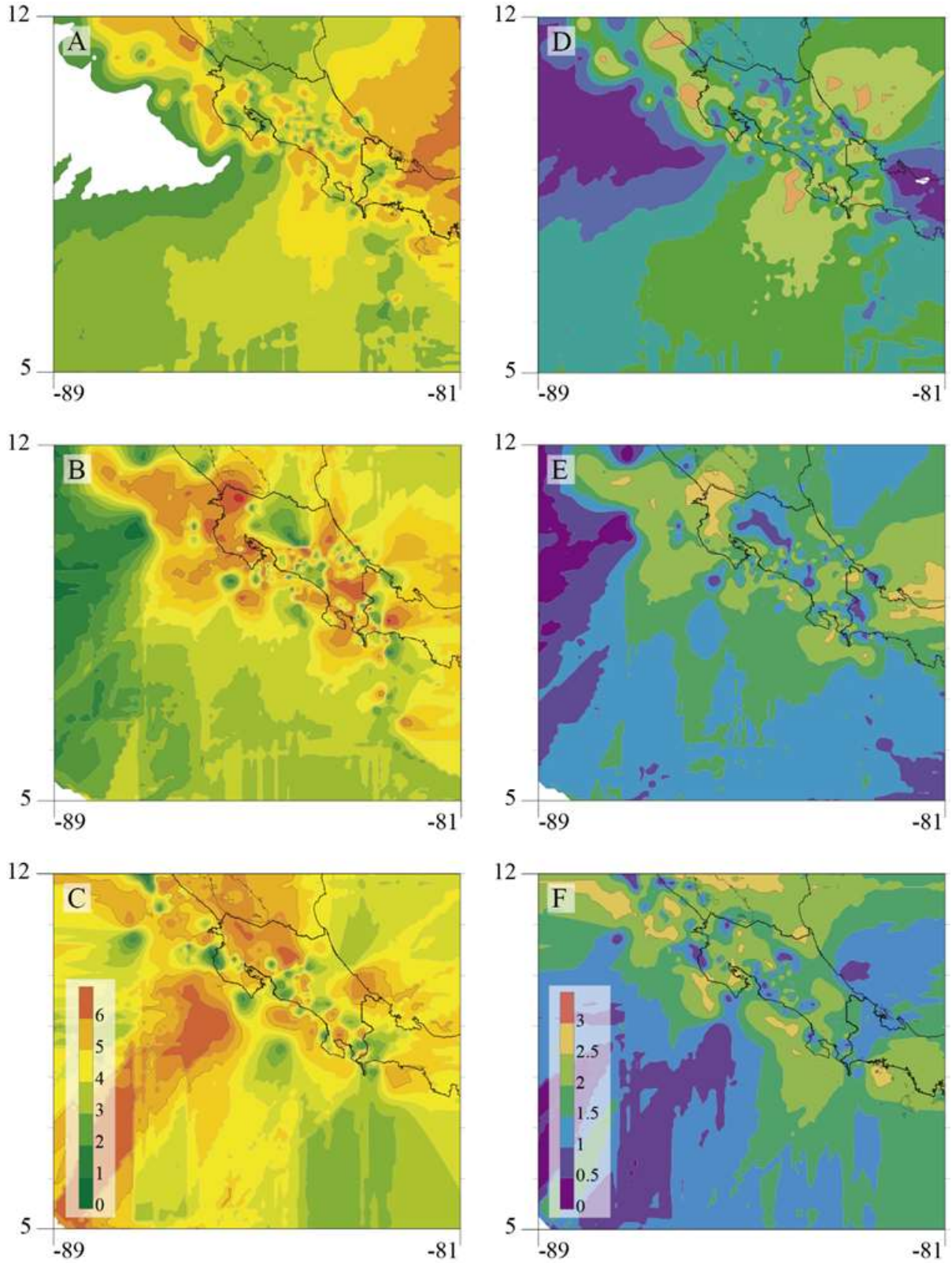

Figure 8. Regional interpolation of the WSM regime code (insets A, B, C) and the R' index (Insets D, E, F) by increasing depth to configure their behaviour across and along the three crust layers. Some important contrast within close distances is observed in the maps explaining local and regional tectonic conducts discussed in the text along with the meaning of both scales.

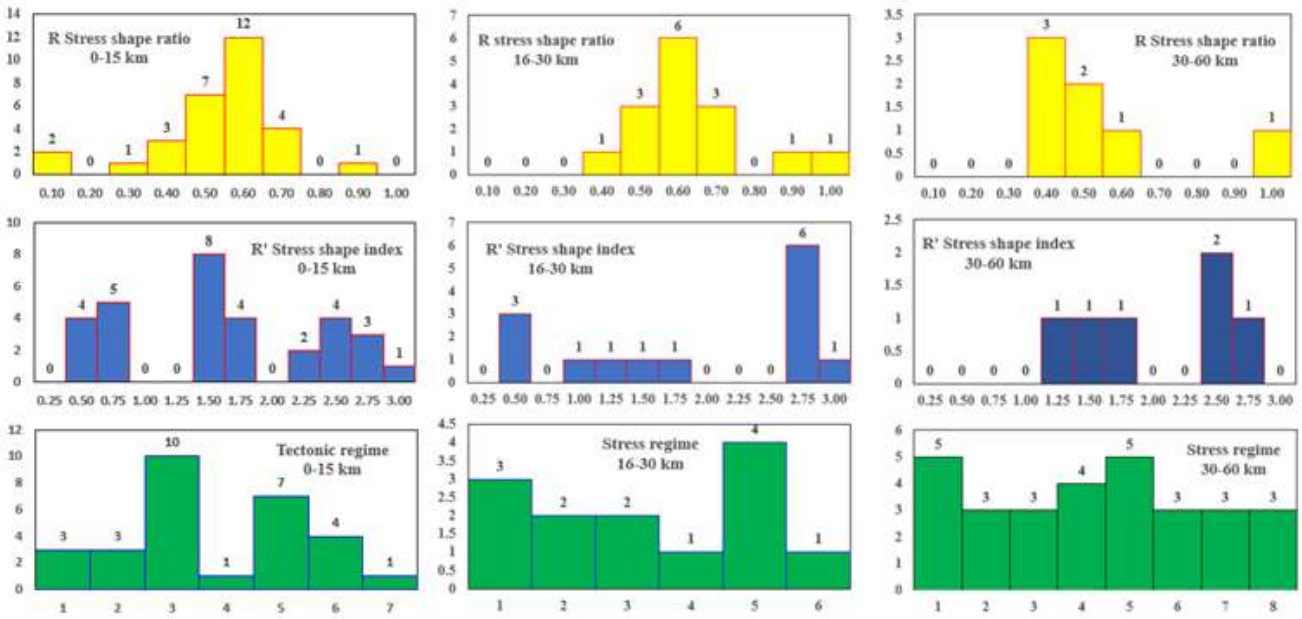

Figure 9. Histograms depicting the range variability of the R, R' and stress regime for every crust layer. Note the strong tendency to permutation in the upper layer with R values deviating from stable values around 0.50 to extreme ones closer to 0 and 1. This condition decreases at depth and is almost absent at the deeper one. The R' values are 0=radial extension, 0.5=uniaxial extension, 1.0= transtension, 1.5=strike-slip, 2.0=transpression, 2.5=uniaxial compression and 3.0 radial compression. The stress regime codes are: Normal faulting =1, transtension= 2, Strike-slip = 3, transpression= 4, Thrusting = 5, and unknown= 6.

It is concluded that the stress field tensors although are of good quality also have a relatively poor stability, especially in the upper layer, and are prone to permutation of their principal axes, allowing the development of a wide variety of faulting regimes, some generated by direct stress and other by stress axes exchange. The respective FM triangular classification plots confirm this property (Figures 2,3). Stress axes permutation may explain partially the time-space vicinity of compressive and extensive features, but such research is implemented in another study.

5.2 The maximum horizontal stress SH Max

It is noticed that only a relatively small amount of the total population of FM were inverted due to lack of adequate concentration within given spatial volumes, conditioned by the relative sparsity of active seismic sources. This partial shortcoming is solved by plotting and interpolating in a continuous 2D space of individual SH Max derived from every FM assuming an acting regional field. This scenario fills the stress gaps among the isolated domains where full tensors were determined and also delineates the overall bearing of the sigma 1 for thrusts and strike-slips and sigma 2 for normal faulting. The Win Tensor program outputs the values of the SH Max and with the assistance of the online Shine application (http://shine.rm.ingv.it/index.phtml) developed Carafa and Barba (2013) and Carafa *et al.* (2015), the interpolation was implemented testing different parameters at every crustal stress layer and selected regions. The concepts of Lund and Townend (2007) were also considered in the calculation of horizontal stress orientations with full or partial knowledge of the tectonic stress tensor.

In Figure 10 the deployed maps present small green, pink and yellow arrows pointing the smoothed trajectories of the respective SH Max and the rose diagrams represents the azimuths of the crude data. Map 10-A corresponds to the shallower crust with a general SH Max trend subparallel to the COP convergence direction, but as shown by the rose of orientations, there also exists a wide dispersion of azimuths.

The black and red arrows in A are the measured and calculated horizontal velocity field vectors calculated from GNSS by Carvajal-Soto *et al*., (2020); which display a remarkable parallelism at almost every region and location with the interpolated SH Max trends, depicting the coherence and kinematic logic, in terms of tectonic blocks activity, of both methods. The two internal panels in B and C denote regions of approximate similar interpolated trends while the variations among them are relatively subtle. The long red line is the MAT (Figure 1) where changes in azimuth are observed and along its strike a sharp contrast coincides with the limit between the rough-smooth sea bottom domains, with more outer-rise distensive FM in the latter and subduction generated events in the former, justifying the denoted behaviour of the horizontal stress. Some amount of rotation is present along the PFZ. The right external panel is a recalculated interpolation with the

same input data at a more local scale, which confirms the above discussed items.

Map B in Figure 10 is the prevailing SH Max orientation within the 16 to 30 km depth interval. The tectonic noise diminishes as shown by the rosette with a relative less deviation of azimuths and a similar general NNE mean trend of the maximum horizontal stress. The right panel reflects the prevailing stress conditions in central Costa Rica at the considered seismogenic depth with some SE small rotations, at the roots of the volcanic edifices, from the NNE trend.

Map C displays important changes respect to the above layers, both at the regional and local configurations. Here the SH Max trend almost N40°E with contortions and rotations in the southern MAT while the black arrows of the raw data as well as the interpolation shows a different stress scenario. It is evident the coincidence of the new condition with the presence of the CVR (Figure 1) acting as a deflector due to the density contrast with the sedimentary and volcanic deposits filling central Costa Rica. It is also clear that the SH Max returns to its general NE trend north of this stress barrier.

From the previous analysis emerges that the detected directional changes of the SH Max are considered to be highly influenced by regional crustal bodies and structures actually covered and hidden by recent deposits eroded from the very active mountain building process and tectonic loading sensu Lee *et al*. (2017). These authors also claim that the crustal stress field may be generally invariant with depth in regions away from the plate boundaries as observed at the Japan and Chile subduction zones and at the India-Eurasia plate boundary. In the present case, the tectonic setting is by far more complex due to the interaction of three main plates in the close vicinity, influencing the whole Costa Rican crust at different magnitudes and intensities, and generating both disperse and localized effects. The overall geomechanical explanation is associated to the presence of locked subducted slabs, elastic rebound, lack or poorly homogeneous rock densities leads to highest variabilities in the vertical stress, lateral buoyancy forces along with slab-surface branching (Loveless *et al*., 2010; Karagianni *et al*., 2015; Ziegler, 2022).

In figures 3, 5, 6 and 7 it is observed that the invariance is not applicable, at least in terms of P and T axes orientation for every given FM, and when compared to the σ1 and σ3 derived from the inversions, a similar conduct is confirmed, although with a smaller but mechanically feasible population. The slight rotations of the SH Max along the N-S regional strike of the PFZ suggest it is a weak and unlocked plate boundary, without important density contrasts which are not able to act as stress deflectors, despite the extreme seismotectonic activity of the area.

5.3 Stress orders and their origin

The modelling of the SH Max, their behaviour and characteristics clearly indicate that in the SW corner of the Caribbean plate there are operating several orders of the stress field as has been demonstrated by the releases of the World Stress Map.

Heidbach *et al.* (2018) have demonstrated with sound data at representative global tectonic domains the existence of plate-scale first-order, regional or second-order and the local third-order stress fields which are controlled by plate boundary forces, intraplate stress sources (mountain belts and glacial rebound) and active faults, local inclusions, detachment horizons and density contrast, respectively. Also, contrary to a now classical view, the absolute plate motion is often not the control of intraplate stress orientation and higher data density reveals rotations by > 40° within < 70 km. Our results tend to confirm this assertion at the local scale. In the context of the region herewith studied the first order is represented by the stress trends imposed by Cocos plate absolute plate motion.

The second order, with high magnitudes boundary forces, is due to the triple interaction of the COCANA plates and the convergence of the COP on the Caribbean plate, with plenty of involved very active and well-developed stresses. This order is a geomechanical product of the interplay of the first one with the Cordilleras backbones and mayor tectonic accidents which act as local deflectors, reorienting the SH Max towards North.

The third order is due to the density contrasts imposed by the trench-arc parallel active volcanic, igneous, and sedimentary ranges in combination with medium to large regional faults and their interactions which act as tectonic stress deflectors. This order is locally represented by northwest oriented abrupt and sharp contortions. All these stress orders interact and overlap laterally and vertically at some extent, producing complex stress scenarios and partitioning.

These properties along with local and regional permutations of the stress ellipsoid explain unexpected local attitudes of the fault regimes with associated neotectonic complications. For example, in the vicinity of the MAT, PFZ, volcanic and geothermal regions in NW Costa Rica, the relation between the associated pore pressure changes and the stress ratio R must be stablished in future works, since it has been found a critical interdependence when its value is smaller or larger than 0.6 (see figures 7, 9). This fact could explain the important permutation detected in those regions where the associated R values are largely close to 0 or 1.

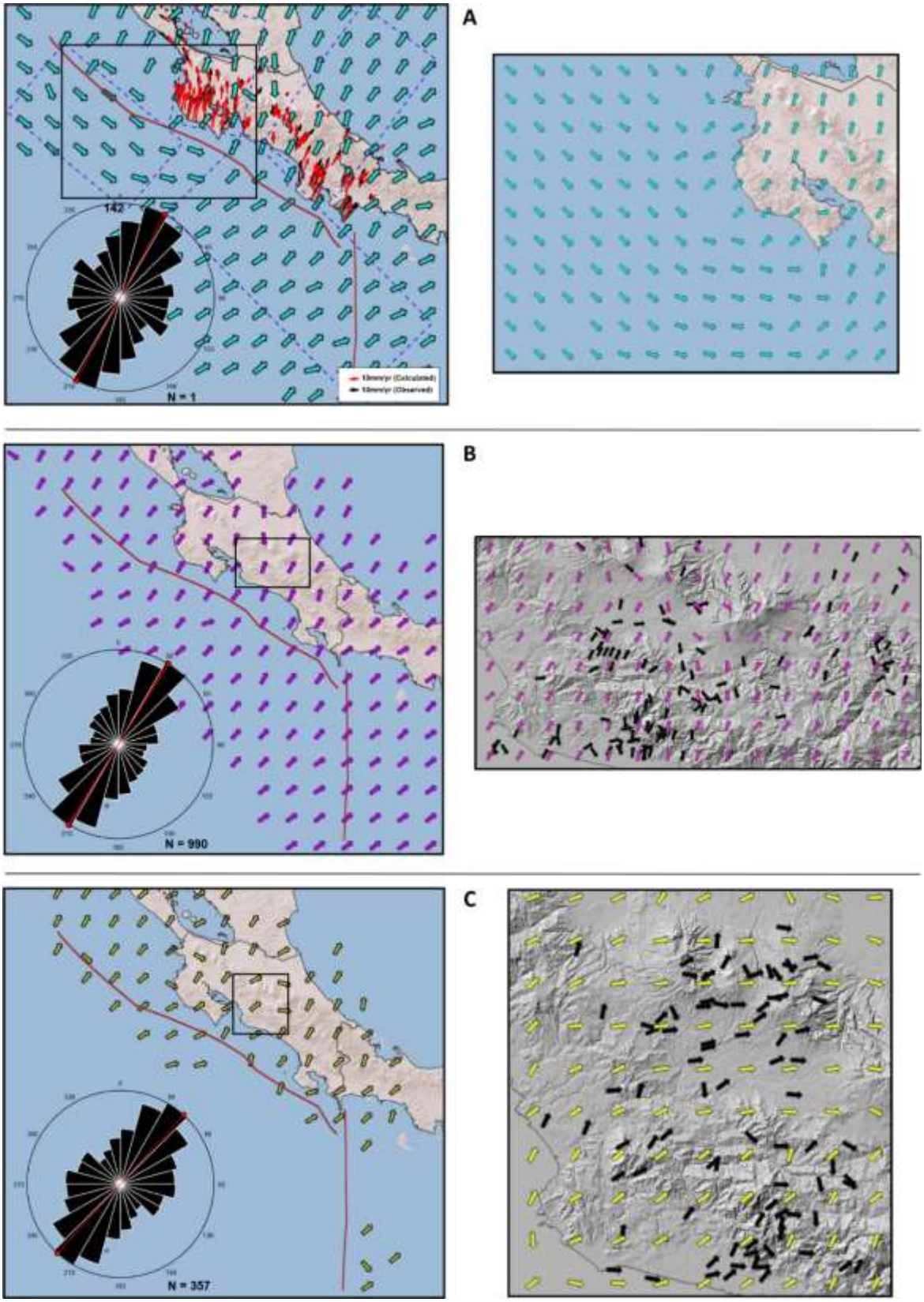

Figure 10. A. The SH Max interpolated trajectories from 1142 FM at the upper crust layer are combined with GPS data of horizontal velocity field by Carvajal-Soto *et al*. (2020). Detailed local interpolation in the right panel highlights SH Max variability and transitions. B and C. Similar integration is done for intermediate and deeper layers. Directional roses depict azimuths of crude data, with mean values marked by a line and dot. MAT and PFZ are indicated by red lines.

5.4 Correlation between the pattern and distribution of the SH Max and crustal elastic deformation based on GNSS observations.

Carvajal-Soto *et al*. (2020) report that the observed velocity field of inter-seismic crustal deformation in Costa Rica is organized into three groups with distinct patterns of behaviour. The northwestern region is characterized by a dominant northward deformation reaching rates of up to 25 mm/yr., which then diminishes and rotates northwestward at rates of up to 12 mm/yr. In contrast, southeastern Costa Rica exhibits deformation moving in the opposite direction, northeastward at rates of up to 40 mm/yr. Meanwhile, the central part displays a diffuse pattern, oriented northward, with deformation rates lower than those observed in the northwestern and southeastern sectors.

The pattern and distribution of the maximum horizontal shear stress (SH Max) obtained from models indicate a consistent northeastward trend. This alignment is in line with the elastic deformation caused by the coupling effects reported by the authors, where high coupling ratios account for more than 70% of the total surface deformation budget in the southeastern Central America Forearc Arch (CAFA) and southwestern Panamá Microplate (PM). Similarly, the SH Max values obtained from models in Central Costa Rica (Figure 10B) align with seismic elastic deformation patterns, with more than 60% of the total surface deformation attributed to coupling effects.

On the other hand, the SH Max values obtained in southwestern Panamá are more consistent with the kinematic rigid motion orientation of the Panamá Microplate (PM), which is eastward. In this region, more than 80% of the surface deformation is attributed to the rigid motion of the PM (Carvajal-Soto *et al*., 2020). Figure 11 summarizes these concepts and the results of the models.

5.5 The Costa Rica stress map

The final product of the previous analysis and discussions is the version of the Costa Rica stress map herewith presented which integrates the properties and characteristics of the acting stress field. It is based on a very representative population of FM solutions and offers a clear picture of the direction and relative magnitudes of the contemporaneous tectonic forces responsible for the ongoing deformation taking place within the SW corner of the Caribbean plate where it interacts with the Cocos and Nazca plates. The López *et al*. (2011) map and the current WSM map 2016 version contain much less data than the one presented here (figure 12) and therefore this work constitutes a contribution to the local and regional knowledge of the tectonic setting and stress database.

In addition, and as an application of the modelling results, the output is a very useful tool to seismic hazard and fault reactivation studies, design of safe underground engineering works, oil and gas exploration strategies and certainly to the extraction of geothermal resources, which are very well developed in the region.

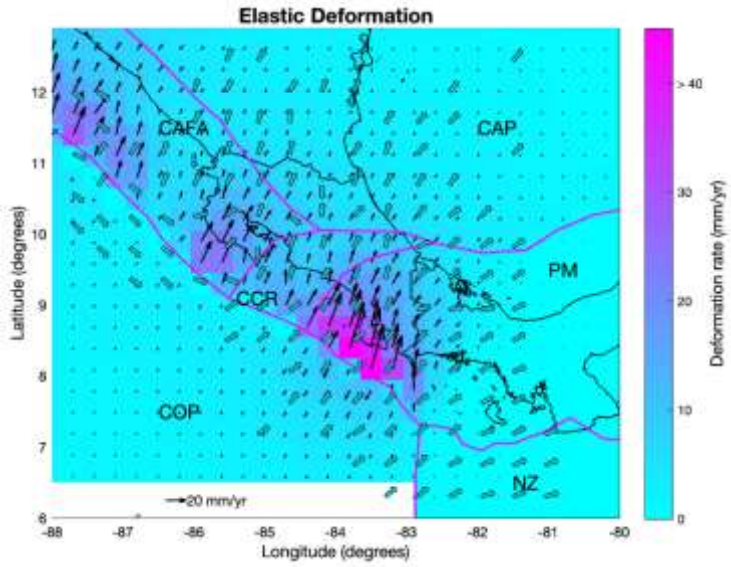

Figure 11. Superposition of SH Max Pattern and Crustal Elastic Deformation based on GNSS Observations reported in Carvajal-Soto et al. (2020). Filled arrows: crustal elastic deformation; thick arrow: SH Max Pattern; CAFA: Central American Fore Arc; CAP: Caribbean Plate; CCR: Central Costa Rica; PM: Panama Microplate; COP: Cocos Plate; NZ: Nazca Plate.

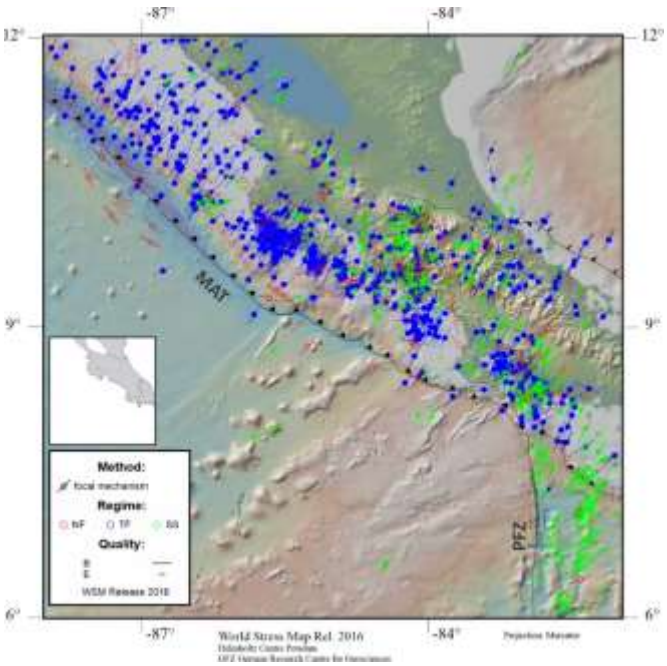

Figure 12. Total stress field map of Costa Rica and surroundings from the database of 2547 focal mechanisms, all depths and magnitudes, presented in this investigation.

6. CONCLUSIONS

The thorough analysis of a very representative population of 2547 focal mechanisms has unveiled the characteristics and properties of the present-day stress field operating in Costa Rica, portions of southern Nicaragua and northern Panamá. The deciphering includes the following findings:

The separation of the database into three crustal layers as from 0 to 15 km depth, 16 to 30 km and deeper than 31 km, has demonstrated to be valid since the stress tensors and the SH Max depict different patterns at each one. The shallower confirms the conclusions of the WSM that good SH Max resolutions are found only within the upper 15 km, although the deeper results are also of very acceptable qualities. The SH Max for each event in association with 86 stress tensors calculated at selected volumes where clusters of FM permit their determination, were used to construct trajectory maps allowing the identification of three orders of stress. The N22°E convergence direction of the Cocos plate is the first order. The second is regulated by the interactions of the triple junction of the Caribbean Plate with the Nazca and Cocos plates in SE Costa Rica, inducing some north oriented rotations from the first order trend up to 30 km depth and +- 20° clockwise rotations. The third order is locally imposed by the cordilleras and their contrasting densities in addition to the regional faults, both acting as stress deflectors with anticlockwise rotations to the N and NW.

The permutation of the stress ellipsoid axes was detected in the 3D Mohr diagrams of some tensors and confirmed as a characteristic property at all crust levels, explaining complex regional fault patterns and interactions. Both the stress regimes and the R' factor are displayed as specific maps for each layer to show their spatial variability.

The contemporary tectonic deformation is controlled by the simultaneous and spatially superposed activity of the compressive and distensive components of the stress field, which is being generated by the overall subduction process and the triple junction of the Cocos-Panamá Microplate-Nazca plates.

The pattern and distribution of the SH Max pointed to northeastward, are consistent with the elastic deformation produced by the coupling effects of the Cocos Plate subduction in southeastern Central America Forearc, western Panamá Microplate and Central Costa Rica, obtained from GNSS observations. This sound correlation confirms the coherence of both methods and the practical potential of their joint application to obtain a consistent model of the contemporaneous regional and local stress-strain scenarios.

The results, when combined with the absolute magnitudes of the stress axes, pave the way to perform more detailed investigations at specific sites and regions for applications. Among them, those related to geotechnics, oil-gas-geothermic exploration and their exploitation designs, hydrotectonics and specially to the evaluation of the slip and dilation tendencies, vital tools for proper seismic hazard evaluations under variable stress scenarios as is the case in the analyzed region.

The results herewith presented, especially those obtained within the volumes associated with subduction and in the surroundings of active volcanoes, do not take into consideration the fluid flow and the thermal regime prevailing in these environments, which in turn directly affect the acting friction. Therefore, they should be incorporated in future research to model the influence of these variables in the local and regional stress field. Also, the ongoing debate and challenging issue, underlined by the WSM, on the strength of plate boundary faults and their low friction coefficient, was giving special care when deriving stress orientations from single focal mechanisms to construct the regional stress maps since their nodal planes are very weak and can display very large differences between the stress axes and the strain axes.

All these findings justify the continuity of this research, incorporating more GNSS data, populations of fault-slips measured at different lithologies, breakout determinations in oil and geothermal wells along with orientation of the Quaternary volcanic vents and dykes, to be integrated into a single stress model. This in turn will be combined with tectonogeomorphic indices of active faulting, which are especially applicable in tropical environments with poor quality of outcrops, to correlate with stress models.

SUPPLEMENTARY MATERIAL

Annex 1. Database of focal mechanisms and moment tensors.
Annex 2. Distribution of depths and magnitudes of the seismic database

FUNDING

This study was supported by DAAD, Universidad Latina de Costa Rica.

DECLARATION OF CONFLICT OF INTEREST

The authors declare that they have no known competing financial interests or personal relationships that could have appeared to influence the work reported in this article.

ACKNOWLEDGMENTS

This research is a contribution to the objectives and database of the World Stress Map, GFZ, Potsdam, Germany and the goals of the ISRM Commission on Crustal Stress and Earthquake. The advice, support and mutual collaboration from O. Heidbach, M. Ziegler. B, Müller, J, Tian and F. Xie is appreciated.

Many colleagues have supported, provided data and inspired this research over the years, among them M. Meschede, W. Frisch, B. Sperner, J. Reinecker, J. Angelier, D. Delvaux, Z. Reches, M.L. Zoback, P. Montone, S. Mora, T. Hergert, M. Schoenball, M. Protti, M. Fernández, W. Rojas, R. Barquero, B. Wolters, R. Quintero, F. Güendel, L. Rojas, G. DeVicente, A. Muñoz, W. Montero, B, Benito, V. Vavryčuk, E.Beauce, A. Garcia, T, Ito, H. Kimura, I. Arroyo, L. Linkimer, P. Denyer, M. Arias, A. Olaiz, G. Alvarado, I. Boschini, L. Madrigal, A. Hidalgo, Y. Álvarez. L. Pérez and N. Wetzler.

Finally, two anonymous reviewers offered their guidance and expertise, and H. Mora played a key role in the implementation of this research.

REFERENCES

Angelier, J. (1975). Sur l'analyse de mesures recueillies dans des sites faillés: l'utilité d'une confrontation entre les méthodes dynamiques et cinématiques. *C.R. Acad. Sci., Paris D281*, 1805-1808.

Angelier, J. (1984). Tectonic analysis of fault slip data sets. *J. Geophys. Res., 89* (B7), 5835-5848.

Arcila, M; Muñoz Martín, A. (2020). Integrated perspective of the present–day stress and strain regime in Colombia from analysis of earthquake focal mechanisms and geodetic data. In: Gómez, J. & Pinilla–Pachon, A.O. (Ed), *The Geology of Colombia, Volume 4 Quaternary*. Servicio Geológico Colombiano, Publicaciones Geológicas Especiales 38, p. 549–569. Bogotá. https://doi.org/10.32685/pub.esp.38.2019.17

Arroyo, I., Husen, S. & Flueh, E.R. (2014). The seismogenic zone in the Central Costa Rican Pacific margin: high-quality hypocentres from an amphibious network. *International Journal of Earth Sciences, 103,* 1747-1764. DOI: 10.1007/s00531-013-0955-8

Arroyo, I. & Linkimer, L. (2021). Geometría de la zona sismogénica interplacas en el Sureste de Costa Rica a la luz de la secuencia sísmica de Golfito del 2018. *Geofísica Internacional, 60*(1), 51-75.

Bangs, N.L., McIntosh, K.D., Silver, E.A., Kluesner, J.W. & Ranero C.R. (2015). Fluid accumulation along the Costa Rica subduction thrust and development of the seismogenic zone. *Journal of Geophysical Research: Solid Earth, 120*, 67-86. DOI: 10.1002/2014JB011265

Bott, M. H. P. (1959). The Mechanics of Oblique Slip Faulting. *Geological Magazine, 96*(2), 109-117. doi:10.1017/S0016756800059987

Bott, M. H. P. & Kusznir, N. J. (1984). The origin of tectonic stress in the lithosphere. *Tectonophysics, 105*(1–4), 1-13.

Camacho, E. (2003). Sismotectónica del extremo norte de la Zona de Fractura de Panamá. *Tecnociencia, 5*(2), 139-152.

Carafa, M; & Barba, S. (2013). The stress field in Europe: optimal orientations with confidence limits. *Geophys. J. Int., 193*(2), 531-548, doi:10.1093/gji/ggt024.

Carafa,M., Tarabusi, G. & Kastelic, V. (2015). SHINE: Web application for determining the horizontal stress orientation. *Computers & Geosciences, 74,* 39-49

Chaves, E., Dubieuf, K., Schwartz, S., Lay, T. & Kintner, J. (2017). Aftershocks of the 2012 Mw 7.6 Nicoya, Costa Rica, Earthquake and Mechanics of the Plate Interface. *Bulletin of the Seismological Society of America, 107*(3), 1227–1239. doi: 10.1785/0120160283

Carvajal-Soto, L. A., Ito, T., Protti, M. & Kimura, H. (2020). Earthquake potential in Costa Rica using three scenarios for the central Costa Rica deformed belt as western boundary of the Panama microplate. *Journal of South American Earth Sciences 97* (2020) 102375

Delvaux, D., Moeys, R., Stapel, G., Melnikov, A. & Ermikov, V. (1995). Palaeostress reconstruction and geodynamics of the Baikal region, Central Asia. Part I. Palaeozoic and Mesozoic pre-rift evolution. *Tectonophysics, 252*, 61-101.

Delvaux, D. & Barth, A. (2010). African stress pattern from formal inversion of focal mechanism data. *Tectonophysics, 482*(1-4): 105-128.

DeMets, C., Gordon, R. G., Argus, D.F. & Stein, S. (1994). Effect of recent revisions to the geomagnetic reversal timescale on estimates of current plate motions. *Geophysical Research Letters, 21*, 2191–2194.

DeMets, C. (2001). A new estimate for present-day Cocos-Caribbean Plate motion: implications for slip along the Central American volcanic arc. *Geophysical Research Letters, 28*(21), 4043-4046.

Güendel, F. (1986). *Seismotectonics of Costa Rica: an analytical view of the southern terminus of the Middle America Trench*. [Ph.D. Thesis]. University of California, Santa Cruz.

Heidbach, O., Reinecker, J., Tingay, M., Müller, B., Sperner, B., Fuchs, K. & Wenzel, F. (2007). Plate boundary forces are not enough: Second and third-order stress patterns

highlighted in the World Stress Map database. *Tectonics, 26*(6), 1-19. DOI: 10.1029/2007TC002133

Heidbach, O., Barth, A., Müller, B., Reinecker, J., Stephansson, O., Tingay, M. & Zang, A. (2016). *WSM quality ranking scheme, database description and analysis guidelines for stress indicator*. World Stress Map Technical Report 16-01, GFZ German Research Centre for Geosciences. http://doi.org/10.2312/wsm.2016.001

Heidbach, O., Rajabi, M., Cui, X., Fuchs, K., Müller, B., Reinecker, J., Reiter, K., Tingay, M., Wenzel, F., Xie, F., Ziegler, M.O., Zoback, M.L. & Zoback, M. (2018). The World Stress Map database release 2016: Crustal stress pattern across scales. *Tectonophysics, 744*, 484-498. https://doi.org/10.1016/j.tecto.2018.07.007

Hu, J. & Angelier, J. (2004). Stress permutations: Three-dimensional distinct element analysis accounts for a common phenomenon in brittle tectonics. *Journal of Geophysical Research Atmospheres, 109*(9), 1-20. https://doi.org/10.1029/2003JB002616

Kassaras, I.G. & Kapetanidis, V. (2018). Resolving the Tectonic Stress by the Inversion of Earthquake Focal Mechanisms. Application in the Region of Greece. A Tutorial. In S. D'Amico (Ed.). *Moment Tensor Solutions. Springer Natural Hazards.* https://doi.org/10.1007/978-3-319-77359-9_19

Karagianni, I., Papazachos, C.B., Scordilis, E.M. & Karakaisis, G.F. (2015). Reviewing the active stress field in Central Asia by using a modified stress tensor approach. *Journal of Seismology, 19*(2), 541-565.

Lee, J., Hong, T-K. & Chang, C. (2017). Crustal stress field perturbations in the continental margin around the Korean Peninsula and Japanese islands. *Tectonophysics, 718*, 140-149.

López, A. (1999). *Neo-and paleostress partitioning in the SW corner of the Caribbean Plate and its fault reactivation potential*. [Ph.D Thesis]. Universität Tübingen, Tübingen, Germany.

López, A., Marshall, J. S., Chinchilla, A.L., Sak, P.B., Chiesa, S., Meschede, M., Alvarado, G. E., Calderón, M., Gazel, E., Villegas, A. & Barquero, R. (2011). *Costa Rica Stress Map: The Sigma Project*. 3rd World Stress Map Conference, GFZ, Potsdam.

López, A. (2012). Andersonian and Coulomb stresses in Central Costa Rica and its fault slip tendency potential: new insights into their associated seismic hazard. *Geological Society (Special Publications), 367*(1), 19-38. DOI: 10.1144/SP367.3

Loveless, J.P., Allmendinger, R.W., Pritchard, M.E. & Gonzalez, G. (2010). Normal and reverse faulting driven by the subduction zone earthquake cycle in the northern Chilean fore arc. *Tectonics, 29*(TC2001), 1-16. DOI:10.1029/2009TC00246

Lund, B. & Townend, J. (2007). Calculating horizontal stress orientations with full or partial knowledge of the tectonic stress tensor. *Geophysical Journal International, 170*(3), 1328-1335. DOI: 10.1111/j.1365246X.2007.03468.x

Marshall, J.S., Fisher, D.M., Gardner, T.W., 2000. Kinematics of diffuse faulting across the western Panama block. *Tectonics, 19,* 468–492

Martínez Garzón, P., Vavryčuk, V., Kwiatek, G. & Bohnhoff, M. (2016). Sensitivity of stress inversion of focal mechanisms to pore pressure changes. *Geophysical Research Letters, 43*, 8441-8450.

McKenzie, D. P. (1969). The relation between fault plane solutions for earthquakes and the directions of the principal stresses. *Bulletin of the Seismological Society of America, 59*(2), 591-601.

Michael, A.J. (1987). Use of focal mechanisms to determine stress: A control study. *Journal of Geophysical Research: Solid Earth, 92*, 357-368.

Montone, P., Mariucci, M.T., Pondrelli, S. & Amato, A. (2004). An improved stress map for Italy and surrounding regions (central Mediterranean). *Journal of Geophysical Research, 109*(B10410), 1-22. DOI: 10.1029/2003JB002703

Montero, W. & Morales, L. D (1990). Deformación y esfuerzos neotectónicos en Costa Rica. *Revista Geológica de América Central, 11*, 69–87.

Morell, K. D. (2016). Seamount, ridge, and transform subduction in southern Central America. *Tectonics, 35,* 357-385. DOI: 10.1002/2015TC003950

Okamoto, K. K., Savage, H. M., Cochran, E. S. & Keranen, K.M. (2022). Stress heterogeneity as a driver of aseismic slip during the 2011 Prague, Oklahoma aftershock sequence. *Journal of Geophysical Research: Solid Earth, 127*(e2022JB024431), 1-15. https://doi.org/10.1029/2022JB024431

Protti, M., Schwartz, S.Y. & Zandt, G. (1996). Simultaneous inversion for earthquake location and velocity structure beneath central Costa Rica. *Bulletin of the Seismological Society of America, 86*(1A), 19-31.

Quintero, R. & Güendel, F. (2000). Stress field in Costa Rica, Central America. *Journal of Seismology, 4*(3), 297-319. DOI: 10.1023/A:1009867405248

Ranero, C.R. & Von Huene, R. (2000). Subduction erosion along the Middle America convergent margin. *Nature, 404*(6779),

748-752.

Saito, T. & Noda, A. (2022). Mechanically coupled areas on the plate interface in the Nankai trough Japan, and a possible seismic and aseismic rupture scenario for megathrust earthquakes. *Journal of Geophysical Research: Solid Earth, 127*(e2022JB023992), 1-15. https://doi.org/10.1029/2022JB023992

Von Huene, R., Ranero, C.R., Weinrebe, W. & Hinz, K. (2000). Quaternary convergent margin tectonics of Costa Rica, segmentation of the Cocos Plate, and Central American volcanism. *Tectonics, 19*(2), 314-334.

Ziegler, M (2022). Rock Properties and Modelled Stress State Uncertainties: A Study of Variability and Dependence. *Rock Mechanics and Rock Engineering, 55*, 4549–4564 https://doi.org/10.1007/s00603-022-02879-8.

Zoback, M. (1992). First- and second-order patterns of stress in the lithosphere: The World Stress Map Project. *Journal of Geophysical Research: Solid Earth, 97*(B8), 11703-11728. https://doi.org/10.1029/92JB00132